© 2020 Wiley-VCH GmbH

ADVANCED
ELECTRONIC
MATERIALS

Supporting Information

for *Adv. Electron. Mater.*, DOI: 10.1002/aelm.202000337

Controlling Defect Formation of Nanoscale AlN: Toward Efficient Current Conduction of Ultrawide-Bandgap Semiconductors

*Yuanpeng Wu, David A. Laleyan, Zihao Deng, Chihyo Ahn, Anthony F. Aiello, Ayush Pandey, Xianhe Liu, Ping Wang, Kai Sun, Elaheh Ahmadi, Yi Sun, Mackillo Kira, Pallab K. Bhattacharya, Emmanouil Kioupakis, and Zetian Mi**

Copyright WILEY-VCH Verlag GmbH & Co. KGaA, 69469 Weinheim, Germany, 2018.

Supporting Information

Controlling Defect Formation of Nanoscale AlN: Towards Efficient Current Conduction of Ultrawide-Bandgap Semiconductors

*Yuanpeng Wu, David A. Laleyan, Zihao Deng, Chihyo Ahn, Anthony F. Aiello, Ayush Pandey, Xianhe Liu, Ping Wang, Kai Sun, Elaheh Ahmadi, Yi Sun, Mackillo Kira, Pallab K. Bhattacharya, Emmanouil Kioupakis, and Zetian Mi**

Section 1. Theoretical computational details

To calculate the defect formation energy in AlN, first-principles density functional theory calculations were performed with the projector-augmented wave method [1, 2] as implemented in the Vienna ab initio Simulation Package (VASP). [3] PBE pseudopotentials (PAW_PBE Al_GW and N_GW_new) [4] were used for Al and N, with a plane-wave cutoff energy of 500 eV to converge the total energy to 1 meV/atom. The HSE06 hybrid density functional [5] with a mixing parameter of 0.33 was employed to obtain a band gap of 6.2 eV for AlN, in close agreement with the experiment. [6] Defect calculations were performed for AlN using 96-atom orthorhombic supercells [7] with a 2×2×2 Γ-centered Brillouin-zone-sampling grid. All structures were relaxed by allowing atoms to move until the force on ions is less than 0.02 eV/Å, with spin-polarization included for unpaired electrons. The defect formation energies were calculated by the following equation:

$$E^f(X^q) = E_t(X^q) - E_t(AlN) + \sum_i n_i\mu_i + q(E_F + E_{VBM}) + E_{corr}.$$

$E_t(X^q)$ denotes the total energy of the supercell with a defect X in charge state q and $E_t(AlN)$ is the total energy of the perfect supercell. n_i is the number of atoms that the supercell exchanges with the chemical reservoir and μ_i is the chemical potentials. E_F is the Fermi energy referenced

to the valence band maximum of the AlN. E_{corr} accounts for the correction to the artificial interaction between charged defect and its image charge. Here, we adopt the approach of Freysoldt *et al*. to evaluate the correction. [8] We assume Mg-rich conditions and μ_{Mg} is bounded by the formation of secondary Mg_3N_2 compound. Our results on defect formation energies and charge-transition levels in AlN are in good agreement with previous theoretical calculations. [9, 10]

Section 2. STEM images of as-grown AlN nanowire *p-i-n* structure

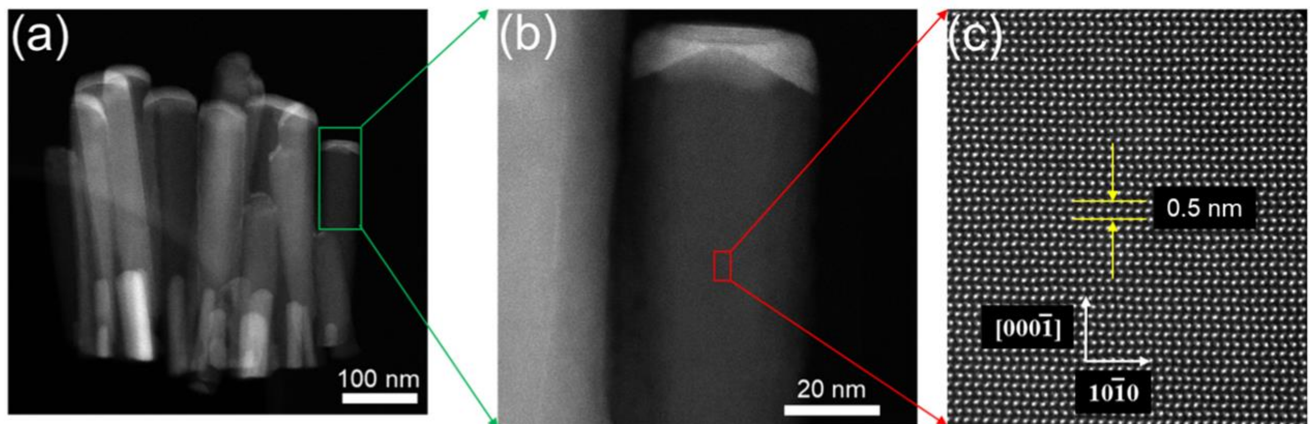

Figure S1. Microstructures of AlN nanowires: (a) Low-magnification STEM-HAADF image showing several AlN nanowires; (b) Magnified STEM-HAADF image shows that the top end of the nanowire outlined in (a) has a thin AlGaN as contact layer; (c) High-resolution STEM-HAADF image taken from the outlined i-AlN active region in (b) showing crystal structure free from dislocations and stacking faults.

Section 3. Configuration-coordinate diagram illustrating optical processes related to Mg dopant and Al vacancy in AlN

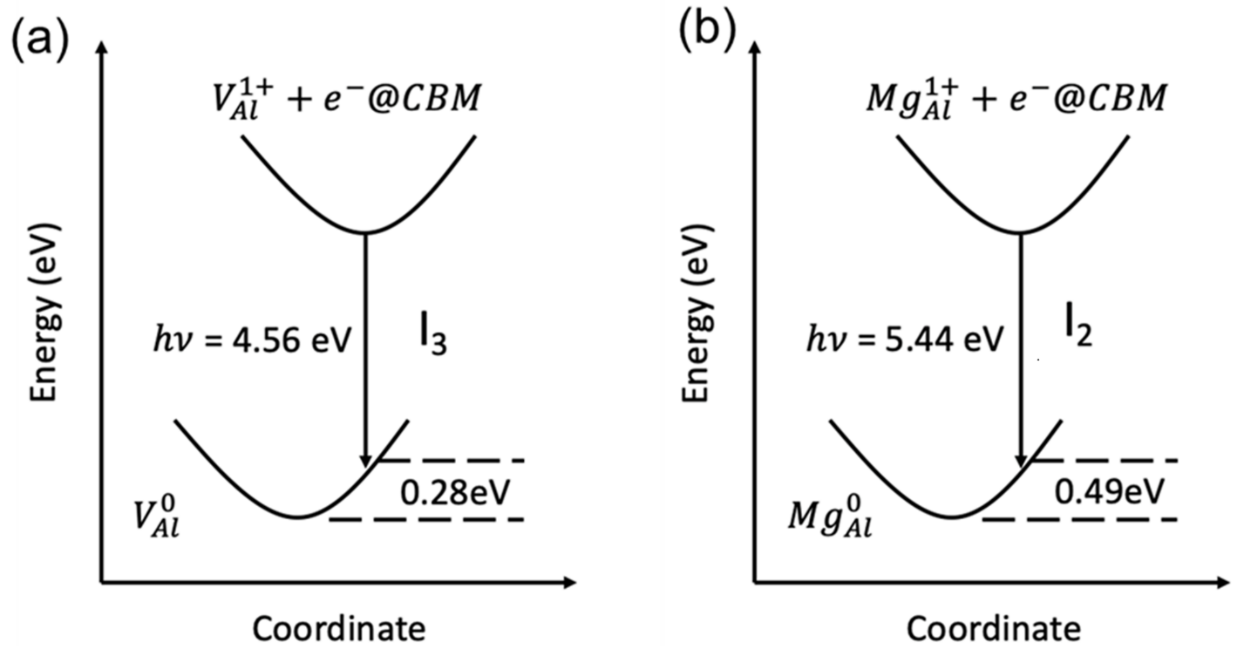

Figure S2. Configuration-coordinate diagram illustrating optical processes related to Mg dopant and Al vacancy in AlN. (a) Recombination of an electron at the CBM with V_{Al}^{1+} to form V_{Al}^{0} leads to an emission peak at 4.56 eV, explaining origin of I_3. (b) Recombination of an electron at the CBM with Mg_{Al}^{1+} to form Mg_{Al}^{0} leads to an emission peak at 5.44 eV, explaining origin of I_2.

Section 4. Non-normalized photoluminescence spectra and intensity ratio of I_2 to I_3 versus the N_2 flow rate

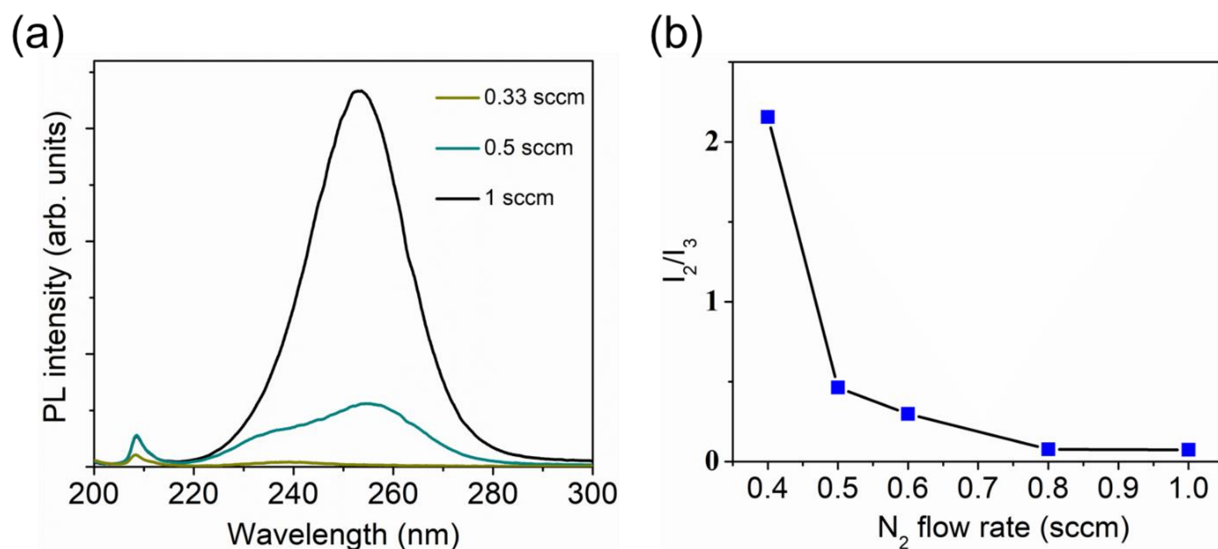

Figure S3. (a) Non-normalized photoluminescence spectra of samples from Group B. All samples were grown at a substrate temperature of 810 °C and Mg BEP of 3×10^{-9} Torr while the nitrogen flow rate was varied among different samples. (b) Intensity ratio of I_2 to I_3 versus the N_2 flow rate derived from photoluminescence spectra of samples from Group B.

Section 5. Eurofins EAG Materials Science secondary ion mass spectrometry (SIMS) depth profile of Mg-doped AlN nanowires grown on Si substrate

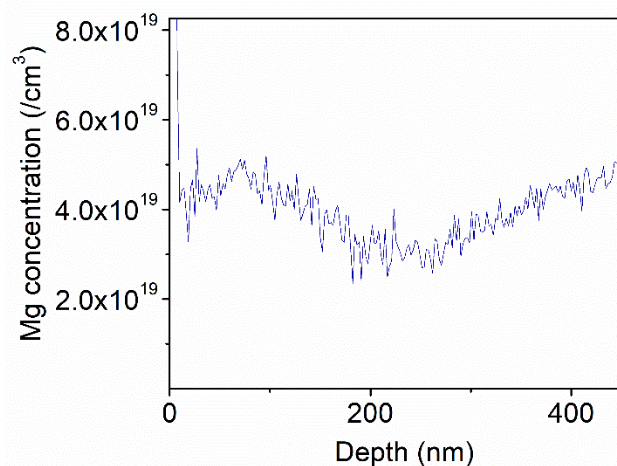

Figure S4. SIMS depth profile of Mg-doped AlN nanowires grown on Si substrate at 865 °C substrate temperature, 1 sccm N_2 flow rate and 7×10^{-9} Torr Mg BEP. A fill factor of 30% for the nanowires was used to derive the average Mg concentration.

Section 6. Photoluminescence spectrum and Gaussian profile analysis of Mg-doped AlN nanowires

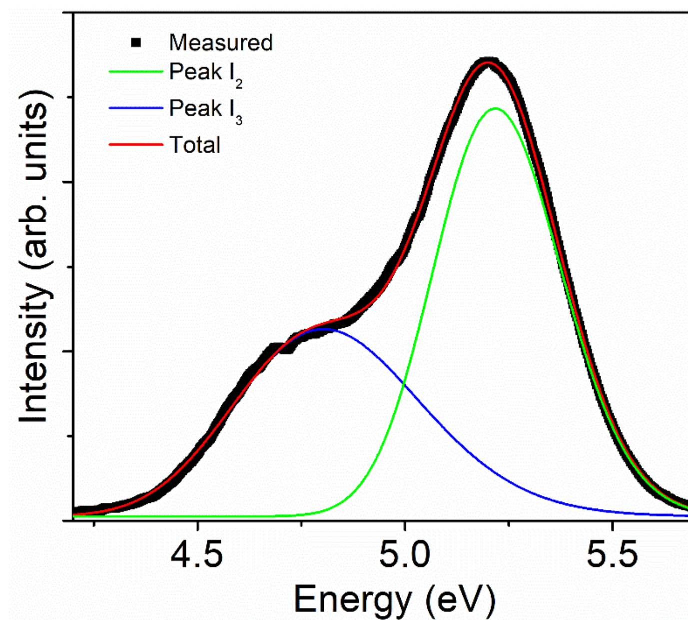

Figure S5. Photoluminescence spectrum and Gaussian profile analysis of Mg-doped AlN nanowires measured under 0.78 W/cm^2 excitation power. The sample was grown under a substrate temperature of 865 ºC, N_2 flow rate of 1 sccm and Mg BEP of 7×10^{-9} Torr.

Section 7. Schematic and electroluminescence spectrum of AlN nanowire-based LED

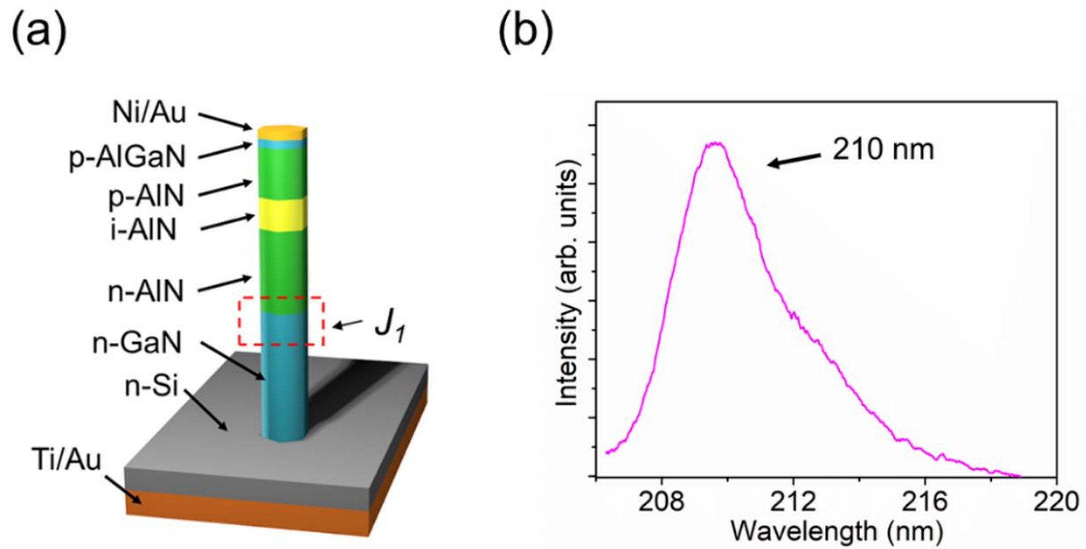

Figure S6. (a) Schematic of AlN nanowire based LED on Si(111) substrate. J_1 points to the heterojunction between *n*-GaN and *n*-AlN. (b) Room-temperature electroluminescence spectrum measured under 30 mA current injection from as-fabricated AlN LEDs.

Section 8. Current-voltage characteristics of *n*-GaN/*n*-AlN unipolar heterojunction

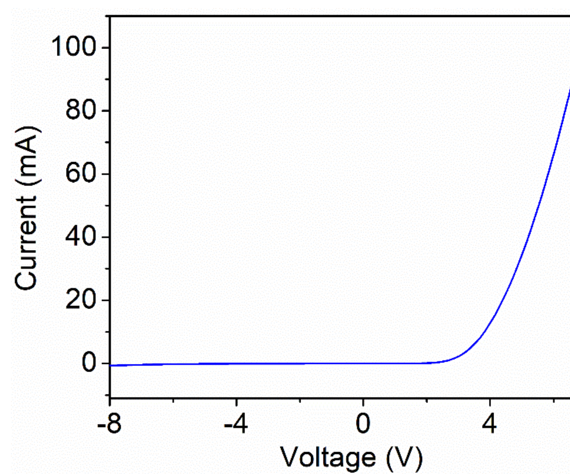

Figure S7. *I-V* characteristics of *n*-type doped unipolar GaN/AlN heterojunction. 80 nm Ti/20 nm Au was used for metal contact with the nanowires.

Table II: Minimum ideality factor and corresponding voltages of AlN nanowire LEDs with different Mg concentrations in the *p*-AlN layer.

	Sample I	Sample II	Sample III
Mg concentration [cm^{-3}]	$1{\times}10^{19}$	$2{\times}10^{19}$	$6{\times}10^{19}$
Minimum ideality factor	14.9	4.6	3.58
Corresponding voltage [V]	3.6	2.4	2.4

Section 9: Analysis of the charge carrier (hole) tunneling process

The hole tunneling process was further explained by calculating the energy band diagram of the AlN *p-i-n* homojunction using two different Mg concentrations as shown in Figure S8. For Mg concentration of $1\times10^{19}/cm^3$, the calculated depletion width into the p-AlN region is ~27 nm. Under equilibrium, despite the Fermi-level is flat throughout the *p-i-n* structure, the built-in potential in the *p*-AlN region causes the band structure as well as the impurity band to bend downwards, wherein the deep level energy states below the Femi-level will be filled by electrons. Under forward bias, these captured electrons can tunnel from one state to adjacent empty states in the valence band, contributing to the tunneling component in Eq. 1 and increasing the ideality factor. When N_A increases to $6\times10^{19}/cm^3$, hole carrier concentration in the valence band increases due to higher Mg concentration and broadened Mg impurity band, leading to a significantly reduced depletion width into *p*-AlN of ~8 nm and a suppressed band bending of *p*-AlN as shown in Figure S8b. As the number of available electrons inside the impurity band reduces, the electron tunneling process is significantly suppressed. It's worth

noting that the deep-level assisted tunneling process will also be suppressed at higher measurement temperature as shown in Figure 4d, wherein hole concentration increases due to a larger portion of ionized Mg-impurities.

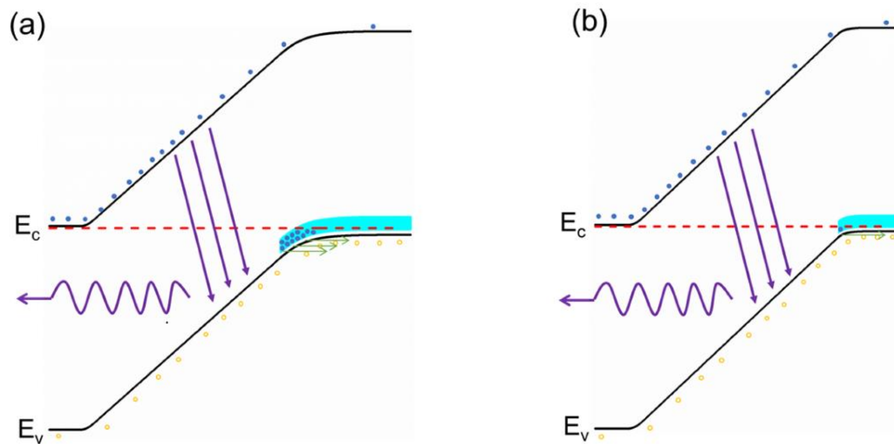

Figure S8. Schematic illustration of the energy band diagram of AlN nanowire *p-i-n* junction with Mg concentration of (a) $1\times10^{19}/cm^3$ and (b) $6\times10^{19}/cm^3$. Mg impurity band bending and deep level assisted electron tunneling process are also illustrated.

Supplementary Reference

[1] P. E. Blöchl, *Phys. Rev. B* **50**, 17953 (1994)

[2] G. Kresse, D. Joubert, *Phys. Rev. B* **59**, 1758 (1999)

[3] G. Kresse, J. Furthmüller, *Phys. Rev. B* **54**, 11169 (1996)

[4] J. P. Perdew, K. Burke, M. Ernzerhof, *Phys. Rev. Lett.* **77**, 3865 (1996)

[5] J. Heyd, G. E. Scuseria, M. Ernzerhof, *J. Chem. Phys.* **118**, 8207 (2003)

[6] H. Yamashita, K. Fukui, S. Misawa, S. Yoshida, *J. Appl. Phys*. **50**, 896 (1979)

[7] C. G. Van de Walle, S. Limpijumnong, J. Neugebauer, *Phys. Rev. B* **63**, 245205 (2001)

[8] C. Freysoldt, J. Neugebauer, C. G. Van de Walle, *Phys. Status Solidi B* **248**, 5, 1067–1076 (2011)

[9] J. L. Lyons, A. Janotti, C. G. Van de Walle, *Phys. Rev. Lett.* **108**, 156403 (2012)

[10] Q. Yan, A. Janotti, M. Scheffler, C. G. Van de Walle, *Appl. Phys. Lett.* **105**, 111104 (2014)